Mössbauer spectroscopy investigation of the *Immm* phase nickelates Gd_2BaNiO_5 and Tm_2BaNiO_5

G. A. Stewart and S. J. Harker
School of Physics, University College, The University of New South Wales, Australian Defence Force Academy, Canberra ACT 2600, Australia

M. Strecker and G. Wortmann
Fachbereich Physik, Universitat–GH Paderborn, D-33095 Paderborn, Germany

(Received 10 August 1999)

The indirect coupling between Ni-O-Ni chains of the *Immm* phase nickelates R_2BaNiO_5 (R=rare earth) results in a range of interesting magnetic behavior. In this work ^{155}Gd Mössbauer spectroscopy data for Gd_2BaNiO_5 (T_N=55 K) are interpreted in terms of a constant electric-field gradient tensor and a temperature-dependent magnetic hyperfine field with a saturation value of 24.5 T. The sensitivity of the spectra to the projection of the hyperfine field enables a magnetic feature at T=24 K to be identified with magnetic reorientation from the *a* to the *b* axis. These results assist with the characterization of the crystal-field interaction for the Tm site in isostructural Tm_2BaNiO_5 (the first such characterization for this particular structural series).

I. INTRODUCTION

The orthorhombic nickelates R_2BaNiO_5 (R=La–Tm,Y) with space group *Immm* are of interest because of their strongly anisotropic crystal structure[1–3] shown in Fig. 1. There is no direct oxygen link between the Ni atoms of neighboring Ni-O-Ni chains running parallel to the *a* axis. Rather, the chains are coupled via the R^{3+} and Ba^{2+} ions. Y_2BaNiO_5 is an example of a weak one-dimensional (1D) antiferromagnetic exchange system with an ordering temperature less than 1.5 K (magnetic order has not yet been observed). The replacement of Y with magnetic rare earths brings about 3D antiferromagnetic order at Néel temperatures which tend to increase with the maximum R^{3+} spin component as shown in Fig. 2.

In the case of Gd_2BaNiO_5, the ordering of the Ni sublattice is not evident from the bulk magnetic susceptibility which increases steadily with decreasing temperature and exhibits a low-temperature anomaly at about 24 K.[3] Instead, the Ni magnetic transition has been observed as a line broadening of the Gd electron-spin-resonance line[4] and via optical spectroscopy.[5] Magnetic susceptibility measurements performed on a single-crystal specimen by Butera *et al.*[4] suggest that the low-temperature anomaly is associated with a reorientation of the magnetization in the *a*-*b* plane. However, on the basis of their optical spectroscopy investigation of Gd_2BaNiO_5 using a dilute concentration of Er^{3+} probes, Popova *et al.*[5] proposed that there is a rotation of the Ni magnetization out of the *a*-*b* plane as the temperature is lowered. The low-temperature magnetic structure for Gd_2BaNiO_5 has not yet been determined using neutron diffraction, presumably because of the high neutron absorption cross section of natural Gd.

In this present work, ^{155}Gd Mössbauer spectroscopy is used to monitor the Gd sublattice magnetism of Gd_2BaNiO_5 over the temperature range 4.2–80 K. With the assistance of a multispectrum analysis program, the data yield both the effective hyperfine field induced at the ^{155}Gd nuclei by the Ni sublattice magnetization, as well as the reorientation of the magnetization with respect to the principal axes of the electric-field gradient (efg) tensor. When combined with ^{169}Tm Mössbauer data recorded for paramagnetic Tm_2BaNiO_5, these results permit the first crystal-field (CF) characterization for this particular isostructural series. The CF characterization suggests an alternative, self-consistent explanation for the optical spectroscopy data obtained by Popova *et al.*[5] A ^{169}Tm Mössbauer investigation of Tm_2BaNiO_5's low-temperature antiferromagnetic phase has already been reported elsewhere.[6]

II. EXPERIMENTAL DETAILS

Polycrystalline specimens were prepared by solid-state reaction of a stoichiometric mixture of Gd_2O_3 or Tm_2O_3

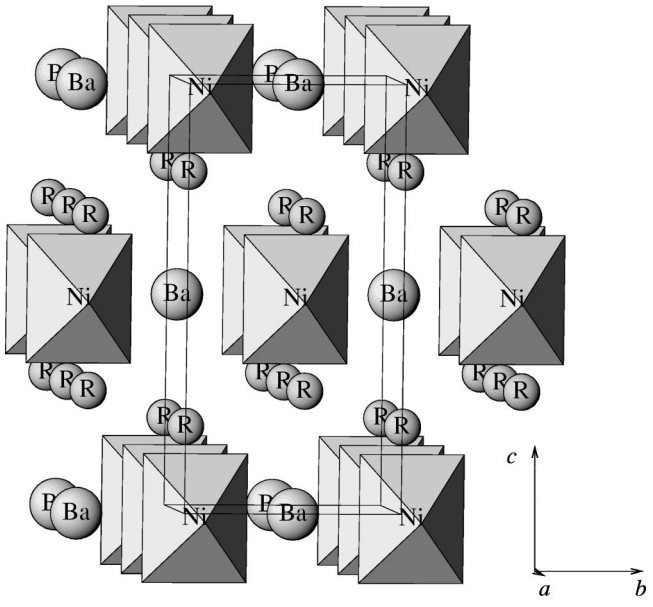

FIG. 1. Structure diagram for R_2BaNiO_5 (space group *Immm*) with the NiO_6 octahedra and Ni-O-Ni chain structure aligned along the *a* axis.

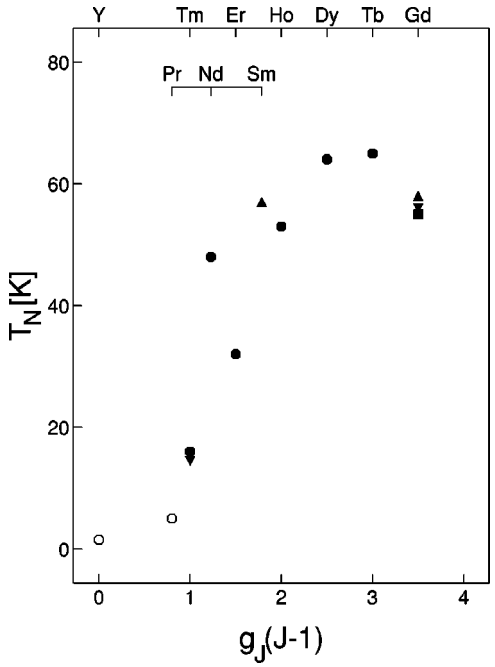

FIG. 2. Néel temperatures for the R_2BaNiO_5 series as a function of the R^{3+} spin component: ● neutron diffraction (Refs. 3, 18, 11, and 19); ▲ optical spectroscopy (Refs. 10 and 5), ▼ Mössbauer spectroscopy (Ref. 6 and this work); ■ ESR (Ref. 4); ○ upper limit. The upper scales indicate the corresponding rare-earth elements.

(99.9%), NiO (99.99%), and analytical grade $BaCO_3$. In the case of Gd_2BaNiO_5, the mix was pressed into pills and calcined at 950 °C for a period of 24 h. During this first stage the carbonate is converted to an oxide and the reaction commences. The pills were then reground and the process repeated a further three times at temperatures of 1050, 1200, and 1200 °C, respectively. X-ray powder diffraction indicated a single-phase specimen with a good quality ($\chi^2 = 1.75$ and $R_{\mathrm{Bragg}} = 6.47$) Rietveld description based on the crystal parameters determined by Amador *et al.*[1] The preparation of the *Immm* Tm_2BaNiO_5 specimen with an estimated 12 wt% Tm_2O_3 impurity phase content is described elsewhere.[6]

The 86.5 keV ($I_g = 3/2$, $E1$, $I_e = 5/2$) ^{155}Gd Mössbauer spectra were acquired using a ^{155}Eu:$SmPd_3$ source which was moved sinusoidally at the same temperature as the rigidly mounted specimen absorber of thickness ≈ 110 mg Gd_2BaNiO_5 cm^{-2}. For the 8.4-keV ($I_g = 1/2$, $M1$, $I_e = 3/2$) ^{169}Tm Mössbauer spectroscopy, a ^{169}Er:$^{168}Er_{0.15}Al_{0.85}$ foil source was mounted externally at ambient temperature and moved sinusoidally. The absorber (≈ 9 mg cm^{-2} of Tm_2BaNiO_5 with CB_4 as a filler) was cooled in a transmission geometry cryostat.

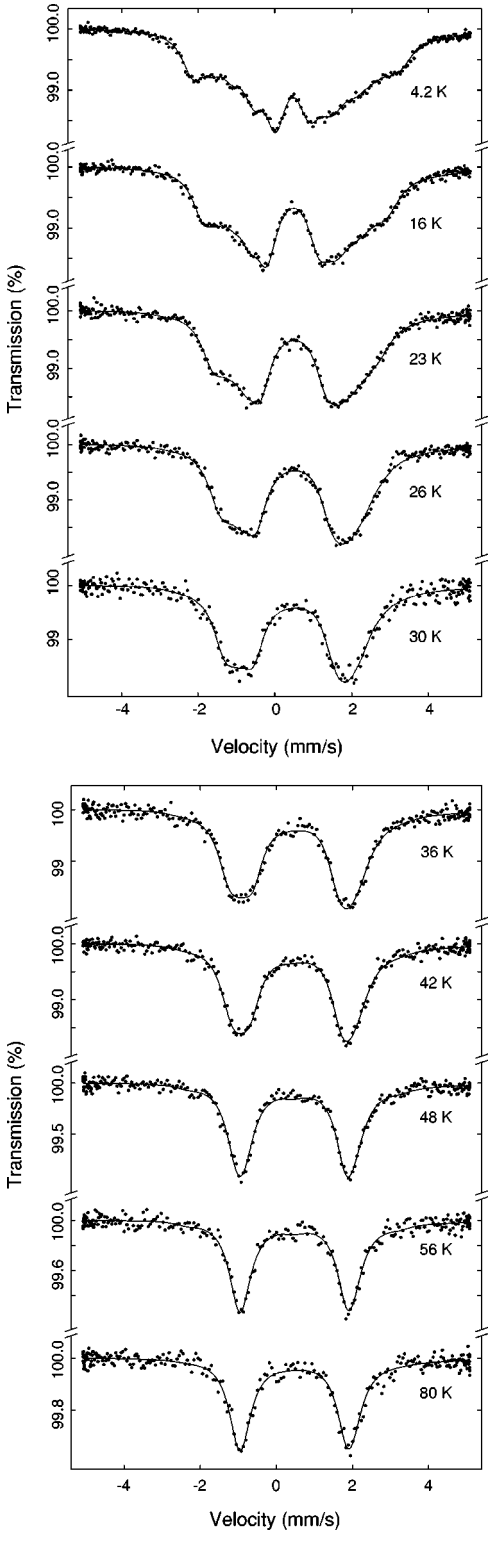

FIG. 3. Representative ^{155}Gd Mössbauer spectra for Gd_2BaNiO_5.

III. RESULTS AND DISCUSSION

A. Gd_2BaNiO_5

Representative ^{155}Gd spectra for Gd_2BaNiO_5 are shown in Fig. 3 as a function of temperature. All spectra could be analyzed in terms of the single Gd site with a full mixed electric quadrupole/magnetic dipole interaction. There was no evidence for additional impurity phases. Because of the thickness of the specimen (estimated at $t \geq 0.7$), the transmission integral approach[7] was employed rather than the usual summation of Lorentzians which is strictly appropriate only for thin absorbers. For this purpose, a natural half width half maximum linewidth of $\Gamma/2 = 0.25$ mm s^{-1} was employed. A multispectra fitting approach[8] was then used to analyze the entire series of spectra simultaneously with the same

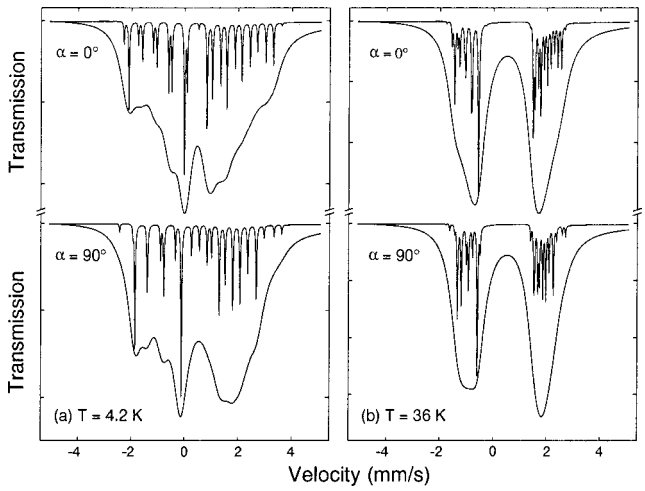

FIG. 4. Simulated ^{155}Gd:Gd_2BaNiO_5 Mössbauer spectra demonstrating the influence of the parameter α, which represents the orientation of B_{eff} projection in the efg tensor's x-y plane [refer to inset in Fig. 5(c)]. The absorption lines with their exaggeratedly narrow linewidths are included to show the position and intensities of the individual hyperfine transitions.

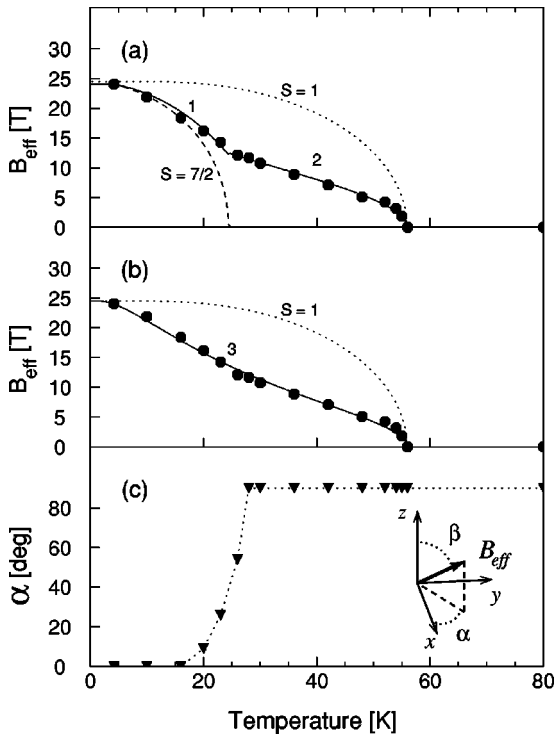

FIG. 5. Key temperature-dependent ^{155}Gd Mössbauer fit parameters for the single Gd site of Gd_2BaNiO_5: (a) effective magnetic hyperfine field B_{eff} with fitted theory (solid lines 1 and 2) which assumes that the Ni sublattice orders at $T_N = 56$ K followed by the Gd sublattice at $T_N^{Gd} = 24.5$ K, (b) the same B_{eff} data with the preferred single transition theory (solid line 3) that ignores the prospect of independent Gd magnetic order, and (c) orientation α of B_{eff} projection in the plane of the x- and y-principal efg axes (see inset). Refer to text for further details of theory curves 1, 2, and 3.

temperature-independent values for the isomer shift δ, the principal electric-field gradient (efg) value V_{zz}, and the asymmetry parameter η. Only B_{eff} and its orientation with respect to the efg axes were allowed to vary. This approach is appropriate because the second-order Doppler effect is small (source and absorber maintained at a similar temperature), and variation of the lattice electric-field gradient (Gd^{3+} is a S-state ion) is expected to be negligible in the absence of structural changes.

For a mixed interaction such as this one, which combines a significant B_{eff} value with an asymmetric efg tensor, ^{155}Gd spectroscopy is particularly well suited to determine both β, the orientation of B_{eff} with the efg z axis and α, the alignment of the B_{eff} projection in the x-y plane [see inset in Fig. 5(c) for angle definitions]. The inclination of B_{eff} to the efg z axis was found to remain constant at a value of $\beta \approx 78°$ over the full temperature range. However, it was necessary to vary the angle α as the temperature decreased through $T = 24$ K. To demonstrate the sensitivity of the ^{155}Gd Mössbauer spectra to α, Fig. 4 shows pairs of theoretical spectra simulated for the values of $\alpha = 0°$ and $\alpha = 90°$ but with all other parameters as fitted for the respective temperatures of 4.2 K [Fig. 4(a)] and 36 K [Fig. 4(b)]. By comparison of these spectra with their counterparts from Fig. 3, it is evident that the angle α varies from 90° to 0° as the temperature is decreased. The fitted temperature-independent parameters are collected in the first row of Table I. The fitted values of B_{eff} and α are shown in Fig. 5 as a function of temperature where the effective hyperfine field is observed to saturate at a value of $B_{\text{eff}} \approx 24.5$ T. This value is considerably smaller than the expected core polarization value of about 30 T and implies the existence of transferred hyperfine fields, most likely originating in the Gd sublattice.

The onset of a nonzero B_{eff} below 56 K is consistent with the T_N values of 55 K (electron spin resonance[4]) and 58 K (optical spectroscopy[5]) reported in the literature. The constant value of $\beta = 78°$ places B_{eff} close to being in the x-y plane of the principal efg axes. This means that the swing from $\alpha = 90°$ to $\alpha = 0°$, observed as the temperature decreases from 30 to 15 K [Fig. 5(c)], corresponds to a reorientation of the local Gd moment from the y- to the x-principal efg axis. Given that Gd^{3+} is an S-state ion with negligible crystal-field influence, it is reasonable to assume that the ^{155}Gd effective hyperfine field will follow the local magnetization. Combined with the single-crystal susceptibility result of Butera *et al.*[4] this implies that the principal efg x and y axes lie in the a-b crystallographic plane.

TABLE I. Temperature-invariant ^{155}Gd Mössbauer parameters for the single Gd site of Gd_2BaNiO_5. For the purpose of comparison, point-charge model (PCM) estimates of the efg parameters are also included.

	V_{zz} [10^{21} V m^{-2}]	η	β [deg]	$\Gamma/2$ [mm s^{-1}]	δ [mm s^{-1}]
Experimental	−10.68(3) [a]	0.40(2)	78(2)	0.35(1)	0.475(6)
PCM $(x,y,z \parallel a,b,c)$					
ligands	−9.9 [b]	0.12			
$r \leq 100a_0$	−10.5 [b]	−0.42			

[a]Deduced using a quadrupole moment of $Q_g(^{155}\text{Gd}) = 1.3$ b (Ref. 16) for ^{155}Gd.

[b]Calculated for $(1-\gamma_\infty) = 61.8$ (Ref. 17).

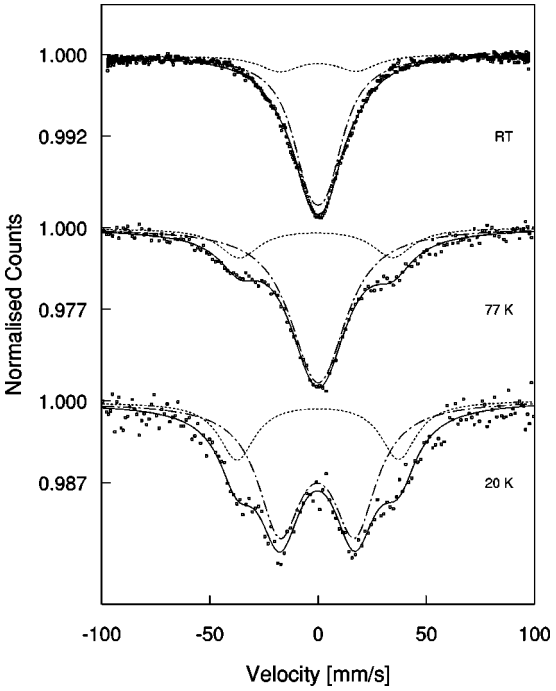

FIG. 6. Representative ^{169}Tm Mössbauer spectra for Tm_2BaNiO_5 above the Néel temperature of $T_N = 14.5$ K.

The temperature dependence of B_{eff} exhibits an inflection at about 24.5 K. Comparison of the data below this temperature with those of the molecular-field theory magnetization curve expected for $S = 7/2$ [dashed line in Fig. 5(a)] suggested that the reorientation process might be associated with magnetic ordering of the Gd sublattice. For these reasons, an initial attempt at modeling the B_{eff} data assumed that the magnetic ordering of the Ni sublattice at $T_N \approx 56$ K was followed by that of the Gd sublattice at $T_N^{\text{Gd}} = 24.5$ K. Assuming that the transferred hyperfine fields acting at the ^{155}Gd nuclei have their origin in the Gd sublattice, B_{eff} is expected to be proportional to the Gd sublattice's reduced magnetization curve according to

$$\sigma = \frac{M}{M(T=0\ \text{K})} = \frac{B_{\text{eff}}}{B_{\text{eff}}(T=0\ \text{K})}. \tag{1}$$

If the Ni sublattice is assigned the spontaneous magnetization curve appropriate for $S = 1$ and assumed not to be influenced by the Gd magnetism, then B_{eff} is described by self-consistent solution of the equation

$$\sigma = B_S\left(\frac{3S}{S+1} \cdot \frac{\sigma \pm \sigma_m}{\tau}\right) \quad \text{for} \quad T \lessgtr T_N^{\text{Gd}}, \tag{2}$$

with $S = 7/2$, $\tau = T/T_N^{\text{Gd}}$, and $\sigma_m = B_m^{\text{Ni}}/B_m^{\text{Gd}}(T=0\ \text{K})$. The molecular fields B_m^{Ni} and B_m^{Gd} acting at the Gd site are those associated with the Ni-Gd and Gd-Gd exchange interactions, respectively. Using this approach the only free parameter is the saturation value of B_m^{Ni} at $T \to 0$ K. The theory curves thus fitted to the experimental data [Fig. 5(a)] correspond to $B_m^{\text{Ni}}(T=0K) = 1$ T for $T \leqslant T_N^{\text{Gd}}$ (curve 1) and $B_m^{\text{Ni}}(T=0\ \text{K}) = 14.1$ T for $T > T_N^{\text{Gd}}$ (curve 2). Because of the large discrepancy between these two values, it was decided that the prospect of an independent ordering of the Gd sublattice could be ruled out.

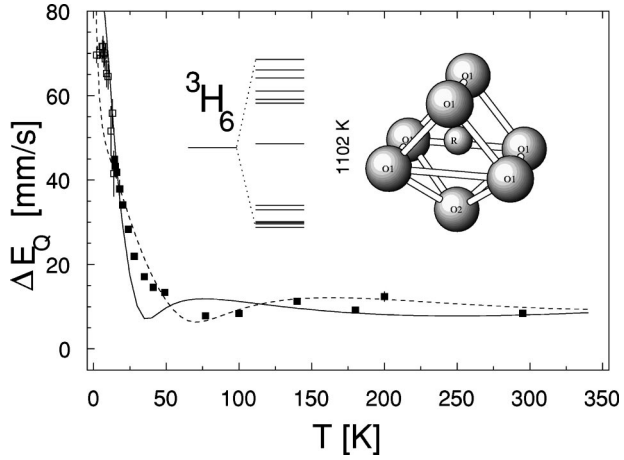

FIG. 7. Quadrupole splitting of the ^{169}Tm $I = 3/2$ nuclear level in the $Immm$-phase of Tm_2BaNiO_5 as a function of temperature. Theory curves refer to preliminary crystal-field analyses with $r_2^2 = -0.4$ (solid line) and $r_2^2 = +0.4$ (broken line). The insets show the Tm^{3+} CF scheme for $r_2^2 = -0.4$ and the arrangement of oxygen atoms surrounding the single R site (c axis vertical and b axis into page).

An alternative approach to model the B_{eff} data assumed the moment at the Gd site to be induced by the Ni-Gd exchange interaction over the entire temperature range. An acceptable description of the experimental data was obtained with $B_m^{\text{Ni}}(T=0\ \text{K}) = 8.4$ T as shown in Fig. 5(b), theory curve 3. This simpler approach is more in keeping with analyses published elsewhere for $R = $ Nd,[9] Er,[10] and Tm.[6] It should be commented that the experimental data just below $T_N \approx 56$ K would be better approximated if a more steeply rising Ni sublattice magnetization curve were adopted, such as implied by direct neutron-diffraction measurements of the Ni moment in Er_2BaNiO_5.[11]

B. Tm_2BaNiO_5

Representative ^{169}Tm Mössbauer spectra for the $Immm$ Tm_2BaNiO_5 specimen are shown in Fig. 6 for temperatures above the Néel temperature of $T_N = 14.5$ K.[6] They are comprised of two quadrupole-split subspectra, one due to the single Tm site of the Tm_2BaNiO_5 and the other due to the Tm_2O_3 impurity. Spectral parameters for the Tm_2O_3 doublet were fixed at those for the single-site interpretation as determined elsewhere.[12,13] At 77 K the doublet with the larger splitting is due to the Tm_2O_3 impurity and the doublet due to the Tm_2BaNiO_5 has sufficiently small splitting that it appears as a broadened singlet. For $T \geqslant 49$ K, it was necessary to fix the linewidth for the Tm_2BaNiO_5 subspectrum to a lower temperature value in order to extract the quadrupole splitting. The quadrupole splitting ΔE_Q thus obtained is given in Fig. 7 as a function of temperature. An unusual feature is the essentially temperature-independent value that persists down to a temperature of about 50 K below which the splitting then increases steeply.

IV. CRYSTAL-FIELD ANALYSIS

As long as the higher electronic terms of a trivalent rare-earth ion can be ignored, the crystal field (CF) perturbation is expressed in terms of a CF Hamiltonian of Stevens operator equivalents $O_n^m(J)$ acting on the ground term manifold with angular momentum quantum number J. For the local orthorhombic C_{2v} (mm) symmetry of the rare-earth site in R_2BaNiO_5, the following simplest form of the CF Hamiltonian is achieved when it is expressed relative to any permutation of axes that align with the crystallographic axes:

$$\mathcal{H}_{CF}=B_2^0O_2^0+B_2^2O_2^2+B_4^0O_4^0+B_4^2O_4^2+B_4^4O_4^4 + B_6^0O_6^0+B_6^2O_6^2+B_6^4O_6^4+B_6^6O_6^6. \quad (3)$$

The crystal-field parameters $B_n^m=\theta_2(1-\sigma_2)\langle r^2\rangle_{4f}A_n^m$ are related to the coefficients A_n^m of expansion of the crystal-field potential in terms of tesseral harmonics.[14] For this local symmetry, the same CF axes serve as principal axes of the efg tensor acting at the rare-earth nucleus. As long as the charge distribution responsible for the CF does not overlap with the $4f$ shell, the total efg tensor components are given by the expressions

$$V_{zz}=-k_{4f}\langle O_2^0(J)\rangle_T-k_{latt}A_2^0 \text{ and} \quad (4a)$$

$$V_{xx}-V_{yy}=-3k_{4f}\langle O_2^2(J)\rangle_T-k_{latt}A_2^2, \quad (4b)$$

where $\langle O_2^0(J)\rangle_T$ and $\langle O_2^2(J)\rangle_T$ are Boltzmann averages of the Stevens operator over the thermally populated CF levels $k_{4f}=(\theta_2e/4\pi\epsilon_0)\langle r^{-3}\rangle_{4f}(1-R_Q)$ and $k_{latt}=4(1-\gamma_\infty)/e$. All other symbols take their usual meaning.[14] The first term in Eqs. (4a) and (4b) represents the temperature-dependent contribution due to the CF distortion of the $4f$ shell and the second term is the constant lattice contribution. The asymmetry parameter η is defined as

$$\eta=\frac{V_{xx}-V_{yy}}{V_{zz}}. \quad (5)$$

All calculations presented below are with the CF axes x, y, and z set parallel to the crystallographic axes a, b, and c, respectively (i.e., x, y, $z\|a$, b, c) and employ the unit-cell description that places the less prevalent of the two oxygen sites at its corners with the rare-earth site labeled as $(4i)$. The lattice parameters and atomic position parameters were taken from the work of Amador *et al.* [R=Gd (Ref. 1)] and García-Matres *et al.* [R=Tm (Ref. 2)]. The inset of Fig. 7 shows the orientation of the seven nearest-neighbor oxygen atoms with respect to crystallographic axes for the two R positions $0,0,z_R$ and $1/2,\ 1/2,\ 1/2+z_R$ (where $z_{Gd}=0.2028$ and $z_{Tm}=0.2033$). For the remaining two R positions $(0,0,\bar{z}_R;\ 1/2,\ 1/2,\ 1/2-z_R)$, the arrangement of oxygen ligands is reflected through a plane parallel to the a-b plane with no change to the CF parameter values.

Because Gd^{3+} is an S-state ion, there is no CF distortion of the $4f$ shell so that the lattice efg components measured at the ^{155}Gd nucleus in Gd_2BaNiO_5 are related directly to the rank 2 expansion coefficients A_2^0 and A_2^2 via the second part of Eqs. (4). Ideal, point-charge model (PCM) estimates of V_{zz} and η were calculated both for the seven nearest-neighbor O^{2-} ligands and for a summation over Gd^{3+}, Ba^{2+}, Ni^{2+}, and O^{2-} point charges out to a range of 100 a_0. The two sets of estimates are included in Table I where they can be compared with the experimental values determined by ^{155}Gd Mössbauer spectroscopy. The absolute magnitudes of PCM calculations must be treated with caution, especially with respect to the long-range rank 2 CF component responsible for the lattice efg contribution. Nevertheless, such calculations have proved to be a useful guide in the case of the 1-2-3-type high-temperature superconductors and related ceramic compounds. In this case, it should be noted that the ^{155}Gd Mössbauer spectrum analysis assumes an arbitrary labeling of the principal axes such that $V_{zz}>V_{yy}>V_{xx}$ and $0<\eta<1$. The fact that both PCM estimates of V_{zz} are in excellent agreement with the experimental value suggests that the assignment of $z\|c$ satisfies this condition. However, the alignment of the principal x and y axes in the a-b plane is less certain. The near-neighbor estimate gives a positive η value which is smaller than the experimental value while the long-range summation gives $\eta=-0.42$ in excellent agreement with the magnitude of the experimental value but of opposite sign. A change in sign of the η value corresponds to a rotation of the principal efg axes through 90° about the z axis.

For isostructural Tm_2BaNiO_5, the quadrupole splitting of the ^{169}Tm, $I_e=3/2$, nuclear level is given by

$$\Delta E_Q=\frac{eQV_{zz}}{4I_e(2I_e-1)}\left(1+\frac{\eta^2}{3}\right)^{1/2}, \quad (6)$$

and is related to the CF Hamiltonian of Eq. (3) via the theory of Eqs. (4), (5), and (6). However, a unique description of the experimental data (Fig. 7) is unlikely to be obtained if all nine CF parameters are allowed to vary independently of one another. In this work, the number of independent rank 4 and rank 6 CF parameters was reduced through PCM computation of the within-rank ratios $r_4^m=B_4^m/B_4^0$ and $r_6^m=B_6^m/B_6^0$. Given the short range of the higher rank crystal-field contributions, only the seven nearest-neighbor oxygen ligands were used for these computations. The calculated ratios are listed in the heading of Table II. Furthermore, the lattice efg parameters determined for isostructural Gd_2BaNiO_5 are readily converted to give estimates of the rank 2 CF parameters for Tm^{3+} in Tm_2BaNiO_5. This gives $B_2^0(Tm^{3+})=3.38$ K and $B_2^2=r_2^2B_2^0$ where $r_2^2=\eta(Gd)=\pm0.4$ (the choice of sign depends on whether the implicit orientation of the experimental ^{155}Gd principal x and y efg axes is the same as that of the CF axes adopted for the ratio calculations or rotated through 90° about the c axis). The only known details of the actual Tm^{3+} CF scheme for Tm_2BaNiO_5 are the energies of the first and second excited CF levels ($\Delta_{10}=E_1-E_0\approx20$ K and $\Delta_{20}=E_2-E_0\approx29$ K, respectively) as determined by Popova *et al.*[15] using optical spectroscopy. As a further constraint, these two energies were included as additional experimental data to be fitted.

Grid-search, least-squares fits of the theory to the experimental ΔE_Q and CF level data were then conducted with the remaining unknown CF parameters, B_4^0 and B_6^0, allowed to vary over the ranges $-300\leqslant B_4^0\leqslant+300$ mK and $-500\leqslant B_6^0\leqslant+500$ μK. The best outcomes are summarized as fits number 1 ($r_2^2=-0.4$) and 2 ($r_2^2=+0.4$) in Table II where the theory values of Δ_{10} and Δ_{20} are shown together with the overall CF splitting Δ_{CF}. From the point of view of the Δ_{10}

TABLE II. CF parameters fitted[a] to the temperature-dependent quadrupole splitting ΔE_Q measured at ^{169}Tm nuclei in Tm_2BaNiO_5. The analyses assume PCM-calculated ratios of $r_n^m = B_n^m/B_n^0 = -13.1$ ($n=4$, $m=2$), -11.9 (4, 4), -9.13 (6, 2), 28.1 (6, 4), and -34.5 (6, 6), and rank 2 parameters converted from the lattice efg results determined for ^{155}Gd in Gd_2BaNiO_5.

Fit number	r_2^2 (^{155}Gd)	B_2^0 [K]	B_4^0 [mK]	B_6^0 [μK]	Δ_{10} [K]/Δ_{20} [K]	Δ_{CF} [K]
1	-0.4	3.38[b]	24.2	-127	23.0/32.7	1102
2	$+0.4$	3.38[b]	43.2	-313	30.5/55.3	1962

[a]Assuming the Tm^{3+} parameter values: $\theta_2 = 0.0101$; $(1-\gamma_\infty) = 59.8$, $(1-\sigma_2) = 0.397$, and $\langle r^2 \rangle_{4f} = 0.59336$ a.u. (Ref. 17); $Q_e(1-R_Q)\langle r^{-3}\rangle_{4f} = -15.2$ b a.u.$^{-3}$ (Ref. 13).
[b]Derived from $V_{zz}(^{155}\text{Gd}) = -10.68 \times 10^{21}$ V m^{-2} for isostructural Gd_2BaNiO_5.

and Δ_{20} agreement, the fit with the negative η is evidently the more reasonable, although this theory curve gives a less desirable description of the data between 25 and 30 K (Fig. 7). Note that the additional ΔE_Q data points (open squares) included in Fig. 7 are for the lower temperature magnetic phase of Tm_2BaNiO_5 ($T_N = 14.5$ K). Since the magnetic spectra were analyzed in terms of an approximate coaxial form of the mixed electric quadrupole/magnetic dipole Hamiltonian[6] these data points represent lower estimates of the true quadrupole interaction and imply that the fit with negative r_2^2 is the more appropriate. The fit with negative r_2^2 also provides a more reasonable value for the total crystal-field splitting Δ_{CF}. The CF scheme corresponding to this fit is included in the inset of Fig. 7. The theory can be forced to fit the ΔE_Q data much more closely by allowing some, or all, of the higher-rank CF parameters to vary independently. However, there is no obvious physical basis for which parameters should be involved in this process. The aim of this preliminary CF characterization is to provide a useful starting point for future refinements made possible by additional experimental data.

V. DISCUSSION

The favored negative sign of the r_2^2 value employed for the above Tm_2BaNiO_5 ΔE_Q data analysis implies that the experimental ^{155}Gd efg parameters for Gd_2BaNiO_5 are with respect to principal axes rotated through 90° compared with the CF axes adopted for PCM calculations of the within-rank CF parameter ratios. Hence the reorientation of the B_{eff} from the *y* efg axis to the *x* efg axis corresponds to a swing of the magnetization from *a* to *b* as the temperature is reduced.

At this stage, it is worth taking a closer look at the susceptibility results of Butera *et al.*[4] for their single-crystal specimen of Gd_2BaNiO_5. As the temperature decreased through 23 K, they observed a sharp increase in susceptibility for $H \| a$ and a sharp decrease for $H \| b$. At first glance, this would appear to correspond to a swing of the magnetization's orientation from the *b* axis to the *a* axis. However, for an antiferromagnet, the susceptibility is larger for *H* applied perpendicular to the magnetization. Working from this assumption, their data imply, instead, that the magnetization swings from *a* to *b* in excellent agreement with the above CF analysis. It is interesting to note that the reorientation transition is much sharper (concluded within a 1-K temperature range) for the single-crystal specimen than it is for the polycrystalline specimens investigated in this work (about 15 K) and by Popova *et al.*[5] who observe complex magnetic behavior over a similar range of about 12 K.

Another test of the present CF analysis is to see whether it offers an alternative explanation of the optical spectroscopy data of Popova *et al.*[5] for dilute Er^{3+} in Gd_2BaNiO_5. Their proposal that the magnetization reorientates from the *a* axis to the *c* axis was directed at explaining the observed collapse of the Er^{3+} ion's ground-state splitting as the temperature was decreased. It is a straightforward exercise to convert the CF parameters from the present work [via the definition following Eq. (3)] and use them to compute Er^{3+} ground-state splittings with a small molecular field applied parallel to the respective crystallographic axis directions. Although the splitting collapses to zero for magnetic alignment with the *c* axis, it is also reduced by a factor of 4 as the magnetization swings from the *b* axis to the *a* axis. Hence, in this sense, a further refinement of the present CF analysis (consistent with a magnetization reorientation from *b* to *a*) may also provide a self-consistent interpretation for the observations of Popova *et al.*

VI. CONCLUSION

Mössbauer spectroscopy measurements of the temperature-dependence of the combined magnetic and quadrupole interaction of ^{155}Gd for Gd_2BaNiO_5 and of the temperature dependent ^{169}Tm quadrupole splitting in the isostructural Tm_2BaNiO_5 are presented. The ^{155}Gd data show the onset of magnetic order for the Ni sublattice at 56 K, consistent with values reported elsewhere[4,5] and, at a lower temperature range, a magnetic reorientation from the *a* to the *b* axis. Based on molecular-field theory modeling of the experimental B_{eff} data, it is concluded that this reorientation is not associated with an independent ordering of the Gd sublattice. The ^{155}Gd interpretation is used to assist with a preliminary crystal-field analysis of the temperature-dependent ^{169}Tm quadrupole splitting, which should provide a useful starting point for future CF analyses of other isostructural compounds.

ACKNOWLEDGMENTS

Our thanks are expressed to Vernon Edge for valuable assistance with the preparation of the specimens. This work was supported by a grant for source irradiation from the Australian Institute of Nuclear Science and Engineering. S. J. Harker acknowledges financial support from University College and the School of Physics.

[1] J. Amador *et al.*, Solid State Ionics **32–33**, 123 (1989).
[2] E. García-Matres *et al.*, Solid State Ionics **63–65**, 915 (1993).
[3] E. García-Matres, J. L. García-Muñoz, J. L. Martínez, and J. Rodríguez-Carvajal, J. Magn. Magn. Mater. **149**, 363 (1995).
[4] A. Butera *et al.*, J. Magn. Magn. Mater. **140–144**, 1681 (1995).
[5] M. N. Popova, I. V. Paukov, Yu. A. Hadjiiski, and B. V. Mill, Phys. Lett. A **203**, 412 (1995).
[6] S. J. Harker, G. A. Stewart, and A. V. J. Edge, Solid State Commun. **100**, 307 (1996).
[7] S. Margulies and J. R. Ehrman, Nucl. Instrum. Methods **12**, 131 (1961).
[8] P. Hettkamp (unpublished).
[9] A. Zheludev, J. P. Hill, and D. J. Buttrey, Phys. Rev. B **54**, 7216 (1996).
[10] G. G. Chepurko *et al.*, Phys. Lett. A **157**, 81 (1991).
[11] V. Sachan, D. J. Buttrey, J. M. Tranquada, and G. Shirane, Phys. Rev. B **49**, 9658 (1994).
[12] R. G. Barnes, R. L. Mössbauer, E. Kankeleit, and J. M. Poindexter, Phys. Rev. **136**, A175 (1964).
[13] G. A. Stewart, R. K. Day, J. B. Dunlop, and D. C. Price, Hyperfine Interact. **40**, 339 (1988).
[14] G. A. Stewart, Hyperfine Interact. **23**, 1 (1985).
[15] M. N. Popova (private communication).
[16] Y. Tanaka *et al.*, Phys. Lett. **108B**, 8 (1982).
[17] R. P. Gupta and S. K. Sen, Phys. Rev. A **7**, 850 (1973).
[18] J. A. Alonso *et al.*, Solid State Commun. **76**, 467 (1990).
[19] E. García-Matres *et al.*, Solid State Commun. **85**, 553 (1993).